Supporting information for

Extremely efficient decomposition of ammonia-N to N_2 using ClO• from reactions of HO• and HOCl generated in situ on a novel bifacial photo-electroanode

Yan Zhang [a], Jinhua Li [a], Jing Bai [a*], Linsen Li [a], Shuai Chen [a], Tingsheng Zhou [a], Jiachen Wang[a], Ligang Xia[b], Qunjie Xu[b,c], Baoxue Zhou [a,c,d*]

[a]School of Environmental Science and Engineering, Shanghai Jiao Tong University, No. 800, Dongchuan Rd, Shanghai 200240, PR China.

[b]College of Environmental and Chemical Engineering, Shanghai University of Electric Power, No.2588 Changyang Road, Shanghai, 200090, PR China.

[c]Shanghai Institute of Pollution Control and Ecological Security, Shanghai, 200092, PR China.

[d]Key Laboratory of Thin Film and Microfabrication Technology, Ministry of Education, Shanghai 200240, PR China.

Contents **Page**

Preparation of WO_3 photoanode. S3

Analytical Methods. S3

Determination of the second-order rate constants S3

Figure S1 Schematic illustration of the preparation of Sb-SnO_2/WO_3. S4

Figure S2 XRD patterns of Sb-SnO_2/FTO. S5

Figure S3 SEM views of the WO_3 layer S5

Figure S4 LSV curves of the WO_3 and WO_3/Sb-SnO_2 anodes S6

* Corresponding authors at: School of Environmental Science and Engineering, Shanghai Jiao Tong University, Shanghai 200240, PR China
E-mail addresses: zhoubaoxue@sjtu.edu.cn (B.X. Zhou); bai_jing@sjtu.edu.cn(J. Bai)

Figure S5	Photoelectrochemical characterization of Sb-SnO_2/WO_3	S6
Figure S6	Degradation of NH_4^+-N by HClO in presence of WO_3	S7
Figure S7	NH_4^+-N degradation using Sb-SnO_2/WO_3 in 50 mM $NaHCO_3$.	S7
Figure S8	Ln(C/C_o) versus time for NB, BA and DMOB degradation.	S8
Figure S9	Model simulated radical concentration in DMOB degradation.	S9
Figure S10	Rate constants of NH_4^+ reacting with ClO•, Cl• and OH•.	S9
Figure S11	Effect of potential NH_4^+-N removal and NO_3^--N generation.	S10
Figure S12	Effects of pH on NH_4^+-N removal and NO_3^--N generation.	S10
Figure S13	SEM of Sb-SnO_2 prepared with different SnO_2 dosages.	S11
Figure S14	Polarization curve of Sb-SnO_2/FTO electrode.	S12
Figure S15	Effect of initial concentration on NH_4^+-N removal.	S12
Figure S16	Formation of chlorate as functions of reaction times.	S13
Figure S17	NH_4^+-N removal in Sb-SnO_2/WO_3 system during five tests.	S13
Figure S18	SEM images of Sb-SnO_2/WO_3 before and after reaction.	S14
Figure S19	Current efficiency and energy consumption as a function of Potential.	S14
Figure S20	Performance Sb-SnO_2/WO_3 for degrading real wastewater.	S15
Figure S21	Illustration of the mechanism in exhaustive denitrification system.	S16
Figure S22	The TN removal in Sb-SnO_2/WO_3 and WO_3 electrode with Pd-Cu/NF as cathode.	S16
Table S1	Second-order rate constants of reaction in the model.	S17
Table S2	Rate constants of scavengers reacting with different radicals.	S17
Table S3	The main characteristics of the real wastewater.	S18

1. Preparation of WO_3 photoanode

In a typical synthesis, 1 g of ammonium paratungstate was dissolved in 93 ml deionized water. 2 mL of concentrated HCl was added to the above solution and stirred. Then 4 ml of H_2O_2 (30%) was added and stirred vigorously for 1 h to dissolve the tungstic acid. Finally, the as-prepared solution was transferred into a 100 mL Teflon-lined stainless autoclave. The FTO substrates were cleaned with ultra-sonication for 15 min in acetone, methanol, and deionized water sequentially. After drying in an N_2 stream, they were placed in a stainless steel autoclave with the conducting side facing down. The autoclave was subjected to heat treatment at 160℃ for 4 h, after which it was cooled to room temperature. The as-synthesized samples were rinsed with a copious amount of deionized water and followed by annealing at 500℃ for 120 min.

2. Analytical Methods.

NB, BA and DMOB were quantified by HPLC (LC-20AT, Japan) coupled with C-18 column (4.6 mm ×150 mm, 5 μm particle size). The mobile phase consisted of water solution (pH 2, adjusted by phosphoric acid) and methanol solution (20:80, v%) at a flow rate of 1.0 mL/min. The concentrations of NB, BA and DMOB were quantified at 266 nm, 227 nm and 230 nm, respectively.

3. Determination of the second-order rate constants between HO•, Cl• and NH_4^+

The second-order rate constants for the reaction of HO• with NH4+ were determined using NB as a reference compound, which reacts with HO• at a second-order rate constant of 3.9×10^9 M^{-1} s^{-1}. The reaction solution was spiked with the mixture of 2 mM NH_4^+ and 2 mM NB. The second-order rate constants was calculated from **Eq. S1**.

$$\ln\left(\frac{[NH_4^+]_0}{[NH_4^+]}\right) = \frac{K_{HO\bullet,NH_4^+}}{K_{HO\bullet,NB}} \times \ln\left(\frac{[NB]_0}{[NB]}\right) \quad \text{(s1)}$$

The second-order rate constants for the reaction of Cl• with NH_4^+ were measured using BA as a reference compound. The solution contained 50 mM Cl^-. BA can react with ClO• rapidly with rate constants of 1.8×10^{10} M^{-1} S^{-1}. BA and NH_4^+ were added into the system at concentrations of 2 mM. NB (10 mM) was used to scavenge the HO• in the system.

$$\ln\left(\frac{[NH_4^+]_0}{[NH_4^+]}\right) = \frac{K_{Cl\bullet,NH_4^+}}{K_{Cl\bullet,NB}} \times \ln\left(\frac{[BA]_0}{[BA]}\right) \quad \text{(s2)}$$

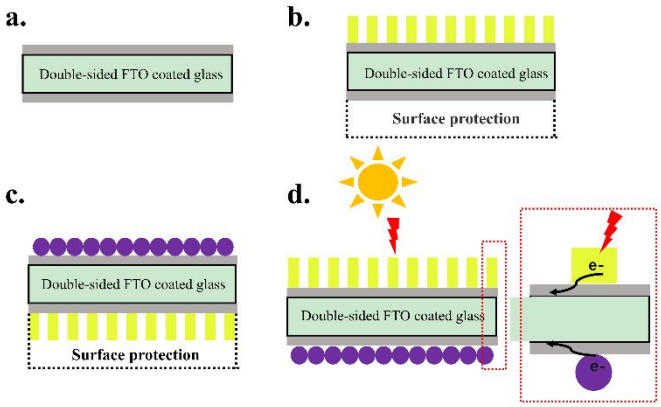

Figure S1 Schematic illustration of the preparation of Sb-SnO_2/WO_3.

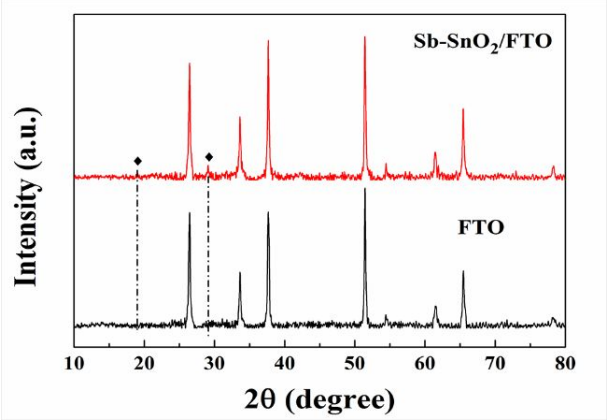

Figure S2 XRD patterns of Sb-SnO_2/FTO.

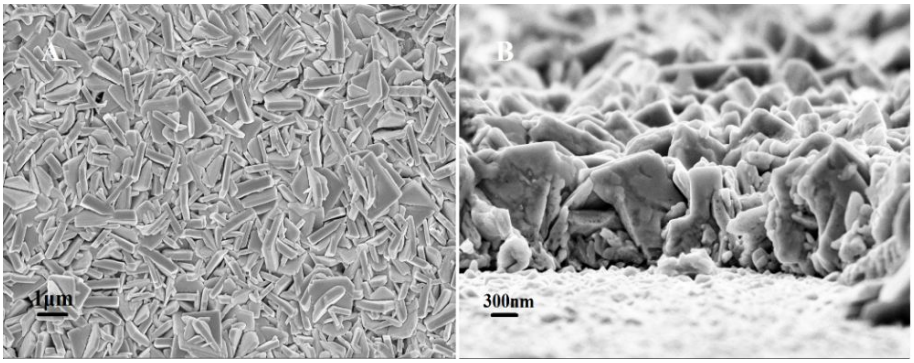

Figure S3 (A) top views of the WO_3 layer (B) cross-sectional views of the WO_3 layer.

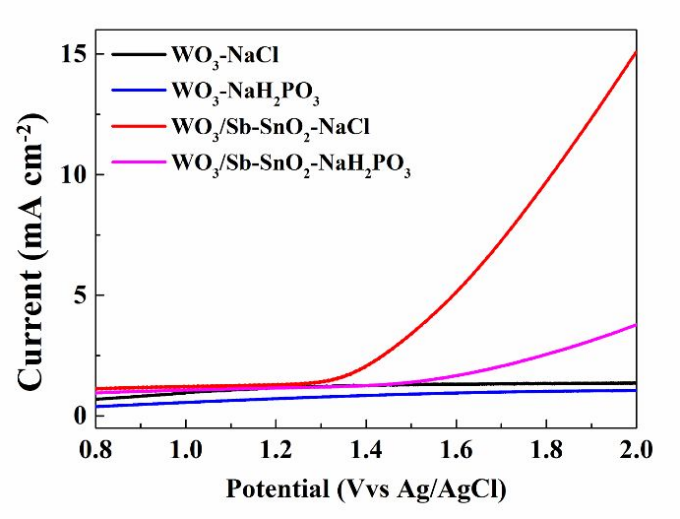

Figure S4 LSV curves of the WO_3 and WO_3/Sb-SnO_2 anodes in NaCl and NaH_2PO_4 solutions.

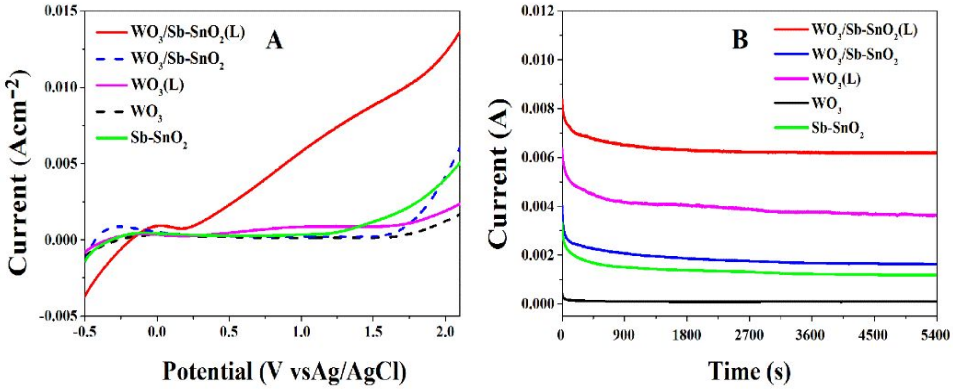

Figure S5 Photoelectrochemical characterization of electrodes in 50 mM NaCl. (A) LSV obtained at a scan rate of 0.05 V s^{-1}. (B) Time profiles of current generation at 1.7 V, respectively. L refers to irradiation.

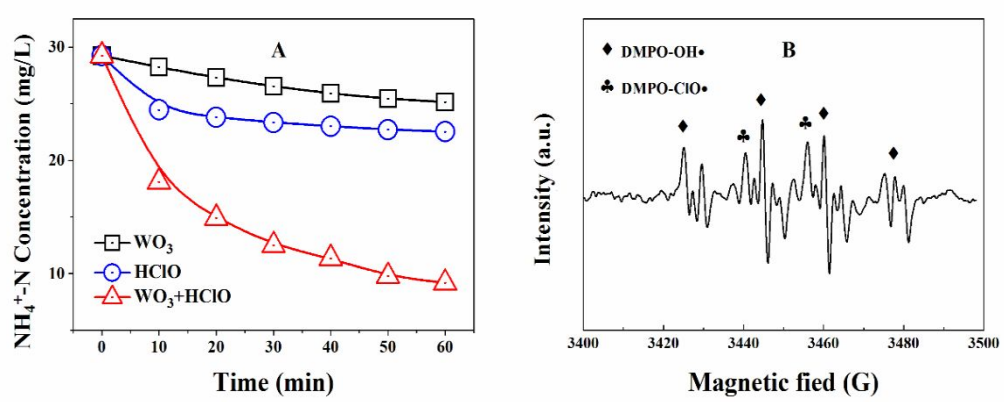

Figure S6 (A) the degradation of NH_4^+-N by HClO in different system. (B) ESR spectra of DMPO−OH• and DMPO−OCl• in this WO_3/HClO system. Conditions: potential 1.7 V vs Ag/AgCl, 30 mg L^{-1} NH_4^+-N, pH=5, NaClO=0.5 g L^{-1} (calculated by free chlorine).

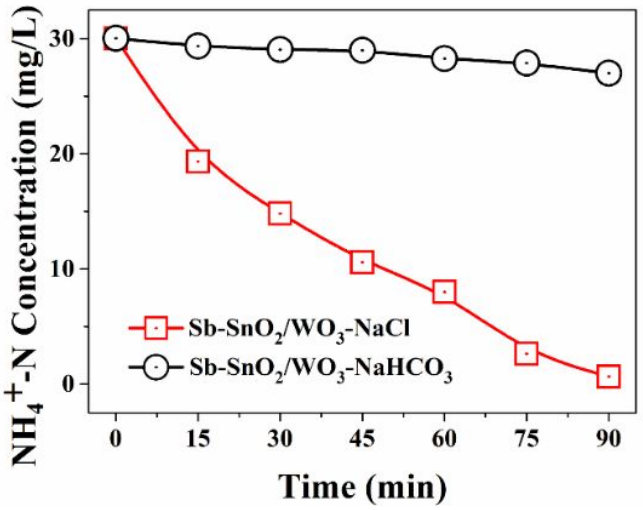

Figure S7 NH_4^+-N degradation using the Sb-SnO_2/WO_3 in 50 mM NaCl and 50 mM $NaHCO_3$ at 1.7 V vs Ag/AgCl.

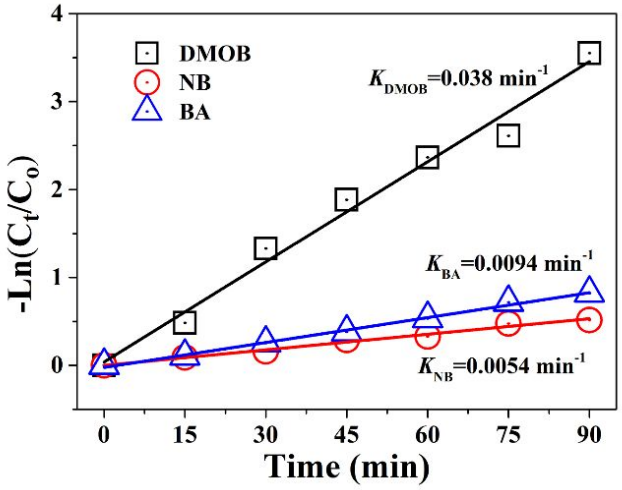

Figure S8 The plots of ln(C/C$_o$) versus time for the NB, BA and DMOB degradation.

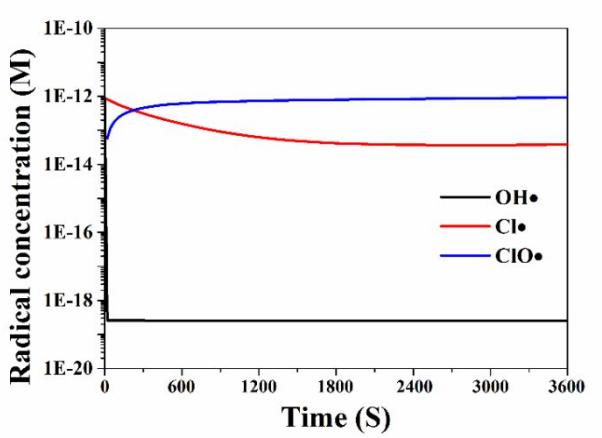

Figure S9 Model simulated radical concentration in DMOB degradation on the Sb-SnO_2/WO_3 operated under 1.7 V vs Ag/AgCl.

In this model, the pH was held constant at 5.0 and the initial NaCl concentration was 0.05M. The concentrations of radical species were calculated during the 60 min reaction time.

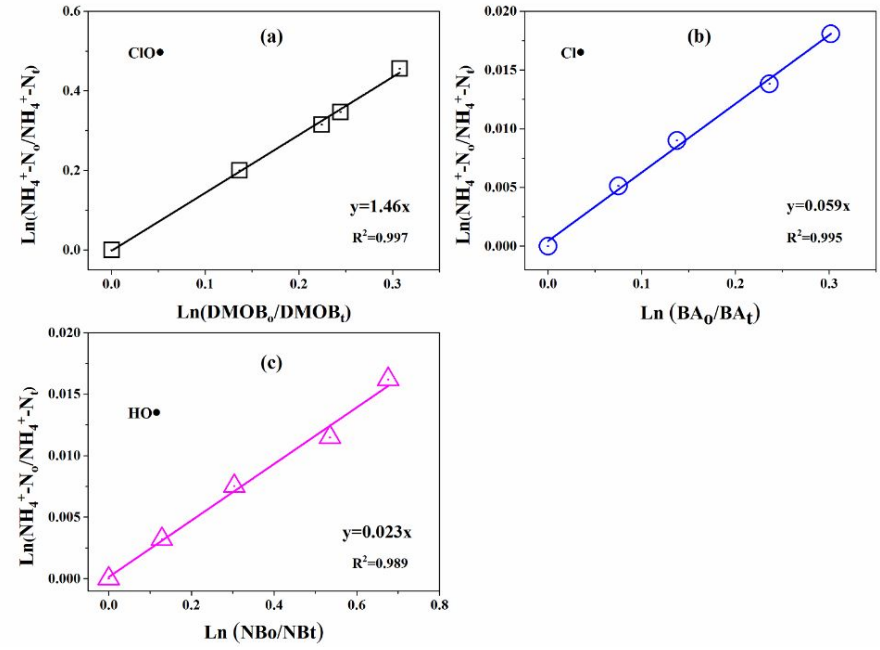

Figure S10 Determination of the second-order rate constants of NH_4^+ reacting with (a) ClO• (b) Cl• and (c) OH• by competition kinetics using DMOB, BA and NB as reference compounds.

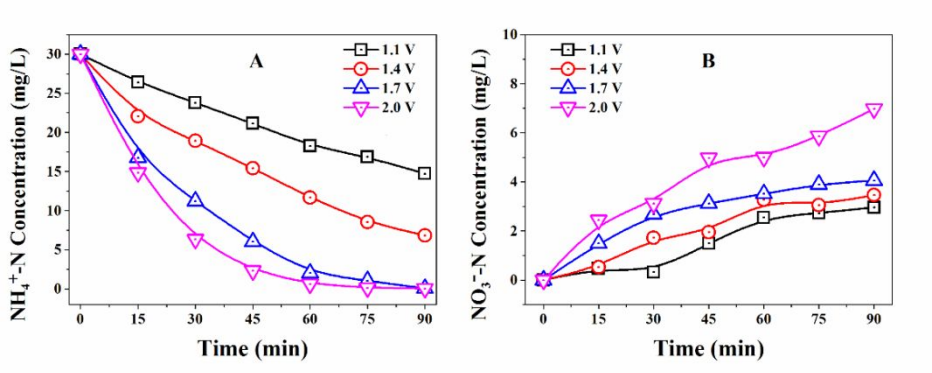

Figure S11 Effect of applied potential on (A) NH_4^+-N removal and (B) NO_3^--N generation. Condition: NaCl 50 mM, pH=5, 30 mg L^{-1} NH_4^+-N.

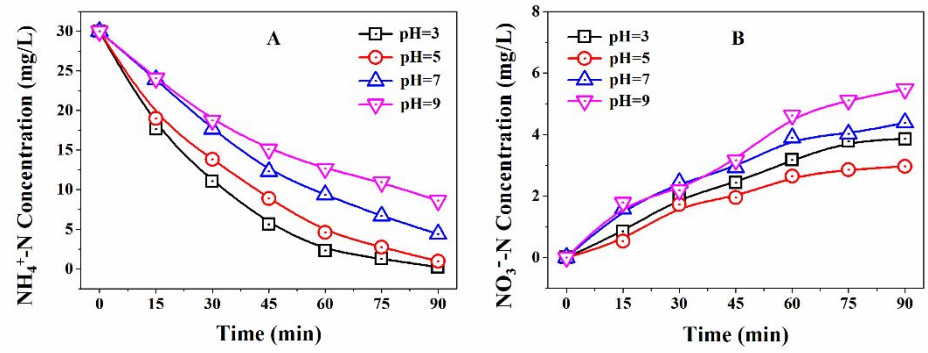

Figure S12 Effects of pH on (A) NH_4^+-N removal and (B) NO_3^--N generation. Condition: NaCl 50 mM, 30 mg L^{-1} NH_4^+-N.

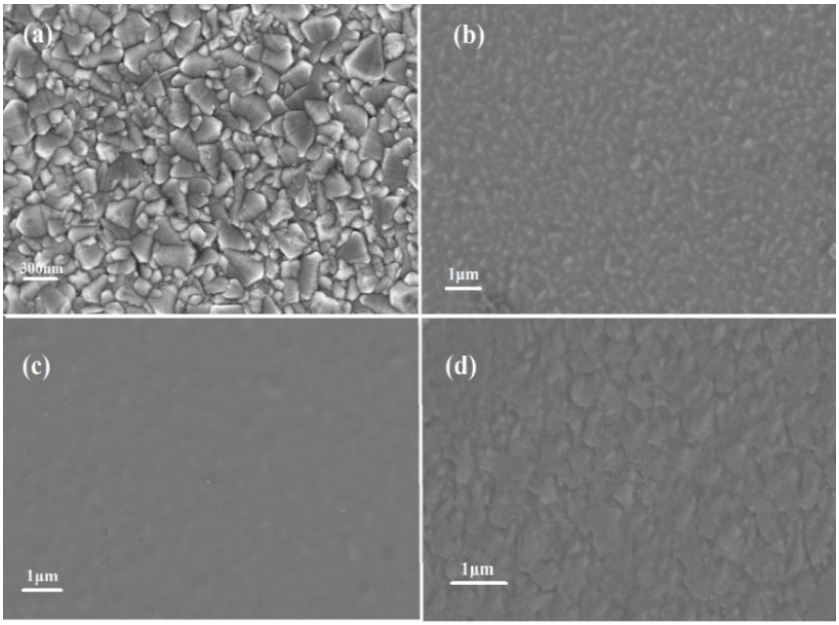

Figure S13 SEM images of Sb-SnO_2/FTO electrode prepared with different SnO_2 dosages of 0 layers (a), 2 layers (b), 6 layers (c), and 10 layers (d).

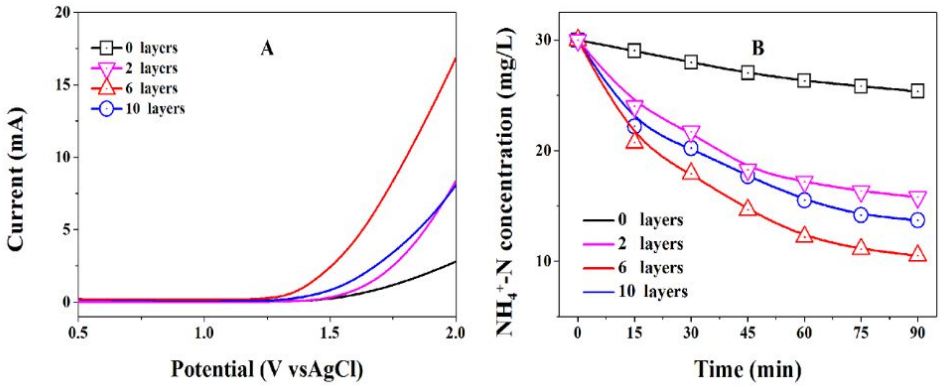

Figure S14 Polarization curve of Sb-SnO_2/FTO electrode (A) and the change of NH_4^+-N concentration in electrochemical degradation (B). Condition: pH=5, 50 mM NaCl, 1.7 V vs Ag/AgCl.

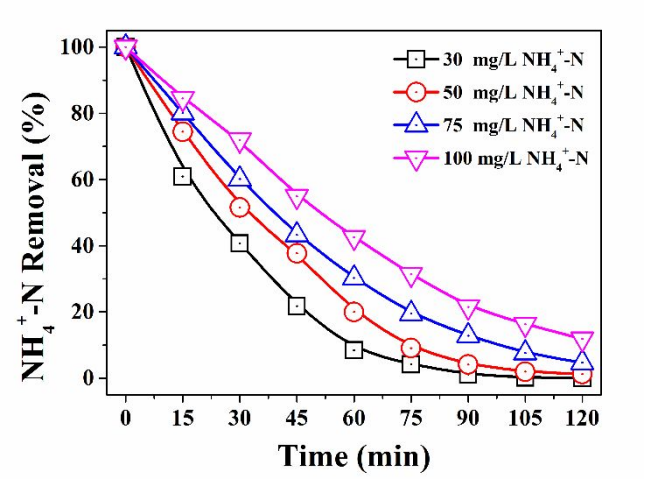

Figure S15 Effect of NH_4^+-N initial concentration on the NH_4^+-N removal efficiencies. Condition: pH=5, potential 1.7 V vs Ag/AgCl, NaCl 50 mM.

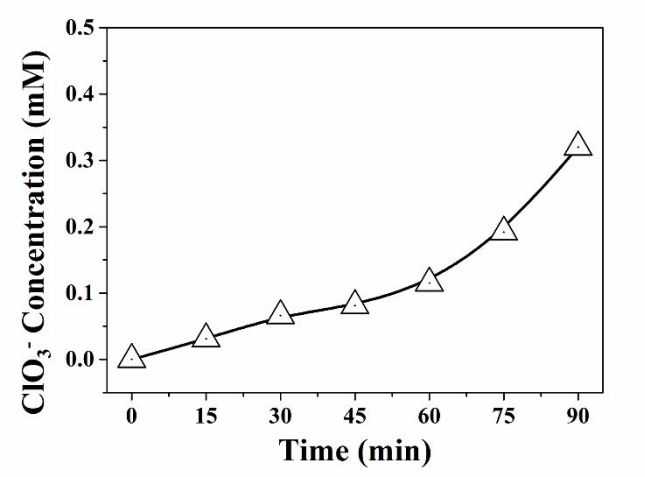

Figure S16 Formation of chlorate as functions of reaction times. Condition: pH=5, 50 mM NaCl, 1.7 V vs Ag/AgCl.

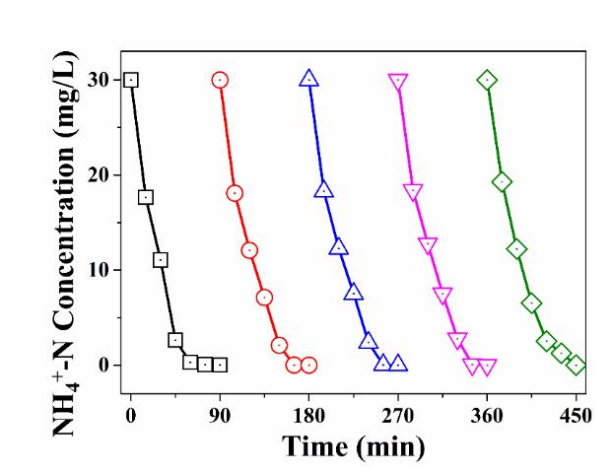

Figure S17 NH_4^+-N removal efficiency in Sb-SnO_2/WO_3 system during five tests at 90 min intervals. Condition: NaCl 50 mM, pH=5, 1.7 V vs Ag/AgCl, 30 mg L^{-1} NH_4^+-N.

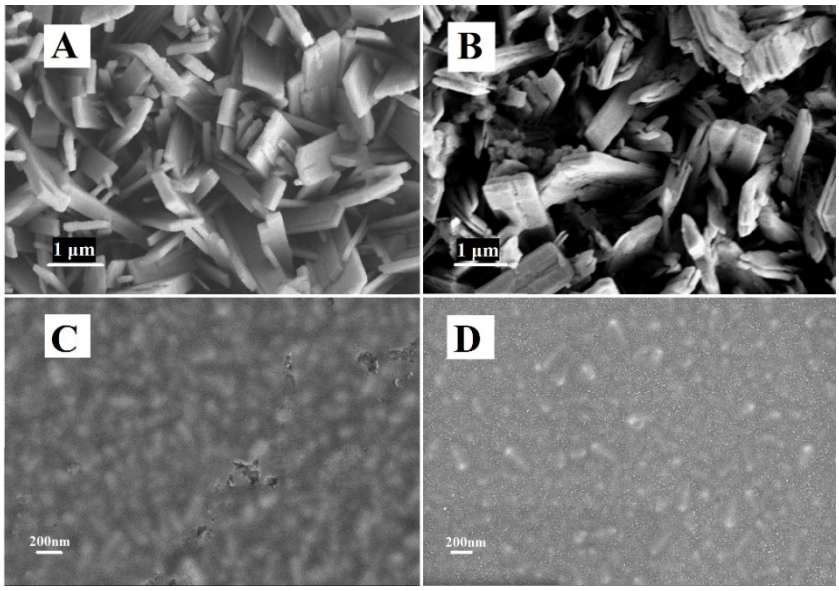

Figure S18 SEM images of prepared WO_3 nanotubes (A) and the used WO_3 nanotubes after the repeated experiments (B), (C) SEM images of prepared Sb-SnO_2 coating and the used Sb-SnO_2 coating after the repeated experiments (D).

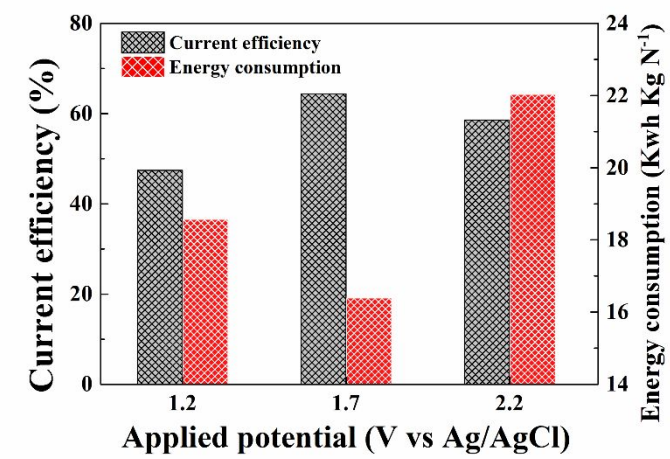

Figure S19 Current efficiency and energy consumption as a function of potential in degrading NH_4^+-N.

Current efficiency can be expressed as:

$$\mathrm{CE} = \frac{n_i \times F \times (C_o - C_t) \times V}{M \times \int_0^t IAdt} \times 100\% \qquad \text{(S3)}$$

where C_o is the initial concentration of NH_4^+-N, C_t is the concentration of NH_4^+-N at

reaction time t (s), V is the volume of the electrolyte (0.05 L), M is the molar mass of NH_4^+ (14 g mol^{-1}), I is the current density (A m^{-2}), A is the effective area of the electrodes (0.0016 m^2), F is the Faraday constant (96485.3 C mol^{-1}) and n is the number of electrons needed for the oxidation of one mole of NH_4^+-N (n=3). The prediction of required ammonia degradation time is obtained when NH_4^+-N concentration decreased below 1 mg L^{-1}.

Energy consumption (kWh kg^{-1} N) is calculated according to Eq. S4:

$$EC = \frac{\int_o^t UIAdt}{3.6 \times (C_o - C_t) \times V} \quad \text{(S4)}$$

where *I* is the current of (A•m^{-2}).

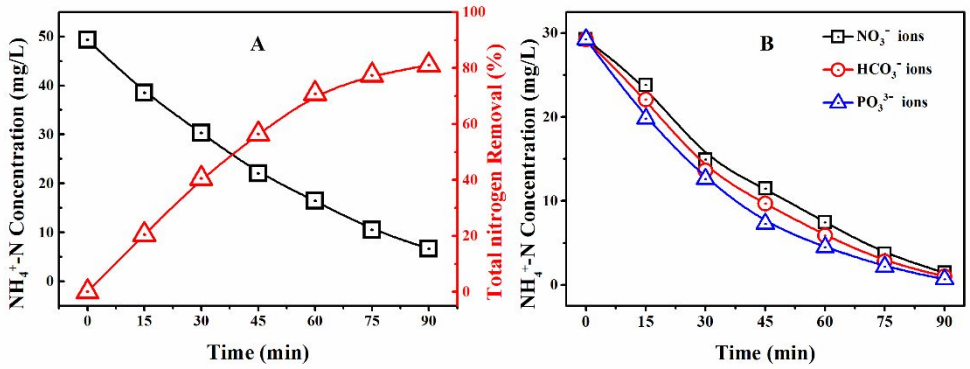

Figure S20 (A) the trends of NH_4^+-N and TN removal efficiency of the Sb-SnO_2/WO_3 degrading real wastewater after filtration. (B) Effects of bicarbonate, nitrate and phosphate ions on the degradation of NH_4^+-N in the Sb-SnO_2/WO_3 system. Conditions: potential 1.7 V vs Ag/AgCl, NaCl 50 mM, 30 mg L^{-1} NH_4^+-N, the concentration of bicarbonate, nitrate and phosphate ions is 2 mM.

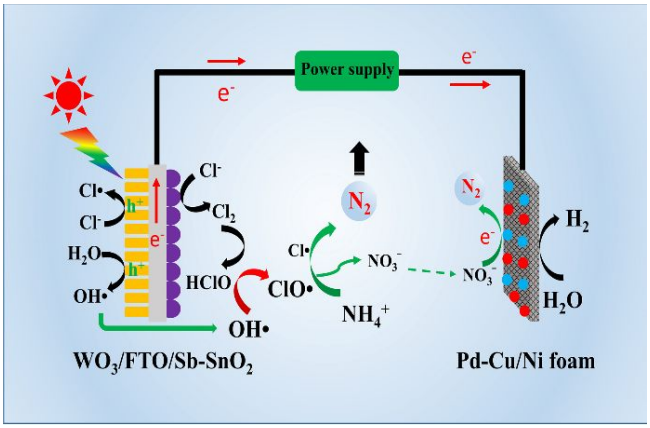

Figure S21 Illustration of the nitrogen removal mechanism in the exhaustive denitrification system.

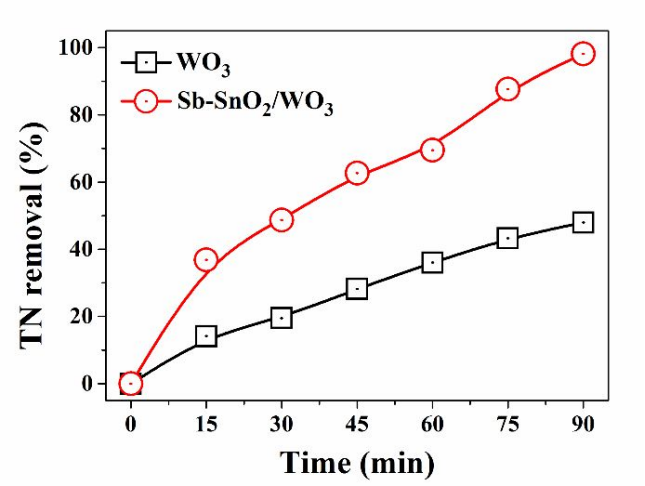

Figure S22 The total nitrogen removal in the Sb-SnO_2/WO_3 and WO_3 electrode with Pd-Cu/NF as cathode. Condition: NaCl 50 mM, pH=5, 1.7 V vs Ag/AgCl, 30 mg L^{-1} NH_4^+-N.

Table S1 Second-order rate constants of reaction in the model

No.	Reaction	Rate constant	References
R1	$H^+ + OH^- \rightarrow H_2O$	1.000E+11	[1]
R2	$H_2O \rightarrow H^+ + OH^-$	1.000E+03	[1]
R3	$OCl^- + H^+ \rightarrow HOCl$	5.000E+10	[1]
R4	$HOCl \rightarrow OCl^- + H^+$	1.600E+03	[1]
R5	$C_2 + H_2O \rightarrow Cl_2OH^- + H^+$	1.500E+01	[2]
R6	$Cl^- + HOCl \rightarrow Cl_2OH^-$	1.500E+04	[2]
R7	$Cl_2OH^- \rightarrow HOCl + Cl^-$	5.500E+09	[2]
R8	$HO\bullet + HO\bullet \rightarrow H_2O_2$	5.500E+09	[3]
R9	$Cl^- + HO\bullet \rightarrow ClOH\bullet^-$	4.300E+09	[3]
R10	$ClOH\bullet^- \rightarrow Cl^- + HO\bullet$	6.100E+09	[3]
R11	$Cl\bullet + OH^- \rightarrow ClOH\bullet^-$	1.800E+10	[3]
R12	$HO\bullet + HOCl \rightarrow ClO\bullet + H_2O$	2.000E+09	[4]
R13	$Cl\bullet + HOCl \rightarrow ClO\bullet + H^+ + Cl^-$	3.000E+09	[4]
R14	$ClOH\bullet^- + H^+ \rightarrow Cl\bullet + H_2O$	2.100E+10	[5]
R15	$ClOH\bullet^- + Cl^- \rightarrow Cl_2\bullet^- + OH^-$	1.000E+05	[4]
R16	$Cl_2\bullet^- + OH^- \rightarrow ClOH\bullet^- + Cl^-$	4.500E+07	[6]
R17	$Cl_2\bullet^- \rightarrow Cl\bullet + Cl^-$	1.100E+05	[5]
R18	$Cl\bullet + Cl\bullet \rightarrow Cl_2$	1.000E+08	[5]
R19	$Cl\bullet + Cl_2\bullet^- \rightarrow Cl^- + Cl_2$	1.400E+09	[5]
R20	$Cl_2\bullet^- + Cl_2\bullet^- \rightarrow 2Cl^- + Cl_2$	8.300E+08	[7]
R21	$Cl_2\bullet^- + HO\bullet \rightarrow HOCl + Cl^-$	1.000E+09	[7]
R22	$OH\bullet + DMOB \rightarrow Product1$	1.800E+10	[7]
R23	$Cl\bullet + DMOB \rightarrow Product\ 2$	2.000E+06	[6]
R24	$ClO\bullet + DMOB \rightarrow Product\ 3$	4.000E+07	[6]

Table S2 Rate constants of scavengers reacting with different radicals

	HO• ($M^{-1}s^{-1}$)	Cl• ($M^{-1}s^{-1}$)	$Cl_2\bullet^-$ ($M^{-1}s^{-1}$)	ClO• ($M^{-1}s^{-1}$)
TBA	6.0×10^8	3.0×10^8	700	
HCO_3^-	8.5×10^6	2.2×10^8	8.0×10^7	N.A.

Table S3 The main characteristics of the real wastewater.

Parameters	Actual wastewater
pH	7.2
NH_4^+-N(mg/L)	50
NO_3^--N(mg/L)	15
Cl^-(mg/L)	132
SO_4^{2-}(mg/L)	40
COD(mg/L)	500
TN	70

References

(1) Matthew, B.; Anastasio, C., A chemical probe technique for the determination of reactive halogen species in aqueous solution: Part 1–bromide solutions. *Atmos. Chem. Phys.* **2006,** *6*, (9), 2423-2437.

(2) Wang, T. X.; Margerum, D. W., Kinetics of reversible chlorine hydrolysis: temperature dependence and general-acid/base-assisted mechanisms. *Inorganic Chemistry* **1994,** *33*, (6), 1050-1055.

(3) Grebel, J. E.; Pignatello, J. J.; Mitch, W. A., Effect of halide ions and carbonates on organic contaminant degradation by hydroxyl radical-based advanced oxidation processes in saline waters. *Environ. Sci. Technol.* **2010,** *44*, (17), 6822-6828.

(4) Hua, Z.; Guo, K.; Kong, X.; Lin, S.; Wu, Z.; Wang, L.; Huang, H.; Fang, J., PPCP degradation and DBP formation in the solar/free chlorine system: Effects of pH and dissolved oxygen. *Water Res.* **2019,** *150*, 77-85.

(5) Guo, K.; Wu, Z.; Shang, C.; Yao, B.; Hou, S.; Yang, X.; Song, W.; Fang, J., Radical Chemistry and Structural Relationships of PPCP Degradation by UV/Chlorine Treatment in Simulated Drinking Water. *Environ. Sci. Technol.* **2017,** *51*, (18), 10431-10439.

(6) Alfassi, Z. B.; Huie, R. E.; Mosseri, S.; Neta, P., Kinetics of one-electron oxidation by the ClO radical. *International Journal of Radiation Applications and Instrumentation. Part C. Radiation Physics and Chemistry* **1988,** *32*, (1), 85-88.

(7) Yang, Y.; Shin, J.; Jasper, J. T.; Hoffmann, M. R., Multilayer Heterojunction Anodes for Saline Wastewater Treatment: Design Strategies and Reactive Species Generation Mechanisms. *Environ. Sci. Technol.* **2016,** *50*, (16), 8780-7.